Geochemistry Geophysics Geosystems G3
AN ELECTRONIC JOURNAL OF THE EARTH SCIENCES
Published by AGU and the Geochemical Society

Article
Volume 9, Number 6
24 June 2008
Q06009, doi:10.1029/2008GC001994
ISSN: 1525-2027

The $^{40}Ar/^{39}Ar$ ages of the sill complex of the Karoo large igneous province: Implications for the Pliensbachian-Toarcian climate change

F. Jourdan
Berkeley Geochronology Center, 2455 Ridge Road, Berkeley, California 94709, USA

Department of Earth and Planetary Sciences, University of California, Berkeley, California 94720, USA

Western Australian Argon Isotope Facility, Department of Applied Geology and JdL-CMS, Curtin University of Technology, G.P.O. Box U1987, Perth, Western Australia 6845, Australia (f.jourdan@curtin.edu.au)

G. Féraud
Géosciences Azur, UMR 6526, CNRS, Université de Nice-Sophia Antipolis, F-06108 Nice, France

H. Bertrand
UMR 5570, CNRS, Ecole Normale Supérieure de Lyon et Université Lyon 1, F-69364 Lyon, France

M. K. Watkeys
School of Geological Sciences, University of KwaZulu-Natal, Westville Campus, Private Bag X54001, Durban 4000, South Africa

P. R. Renne
Berkeley Geochronology Center, 2455 Ridge Road, Berkeley, California 94709, USA

Department of Earth and Planetary Sciences, University of California, Berkeley, California 94720, USA

[1] Reliable geochronological results gathered so far (n = 76) have considerably constrained the timing of the emplacement of the Karoo large igneous province (LIP). Yet strikingly missing from this dating effort is the huge southern sill complex cropping out in the $>0.6 \times 10^6$ km^2 Main Karoo sedimentary basin. We present 16 new $^{40}Ar/^{39}Ar$ analyses carried out on fresh plagioclase and biotite separates from 15 sill samples collected along a N–S trend in the eastern part of the basin. The results show a large range of plateau and miniplateau ages (176.2 ± 1.3 to 183.8 ± 2.4 Ma), with most dates suggesting a ~3 Ma (181–184 Ma) duration for the main sill events. The available age database allows correlation of the Karoo LIP emplacement with the Pliensbachian-Toarcian second-order biotic extinction, the global warming, and the Toarcian anoxic event (provided that adequate calibration between the ^{40}K and ^{238}U decay constant is made). The mass extinction and the isotopic excursions recorded at the base of the Toarcian appear to be synchronous with both the increase of magma emission of the Karoo LIP and the emplacement of the sills. The CO_2 and SO_2 derived from both volcanic emissions as well as carbon-rich sedimentary layers intruded by sills might be the main culprits of the Pliensbachian-Toarcian climate perturbations. We propose that the relatively low eruption rate of the Karoo LIP is one of the main reasons explaining why its impact on the biosphere is relatively low contrary to, e.g., the CAMP (Triassic-Jurassic) and Siberia (Permo-Triassic) LIPs.

Components: 11,734 words, 7 figures, 1 table.

Keywords: $^{40}Ar/^{39}Ar$ ages; large igneous province; Karoo; sill complex; climate change; Pliensbachian-Toarcian.

Index Terms: 1115 Geochronology: Radioisotope geochronology; 0370 Atmospheric Composition and Structure: Volcanic effects (8409); 9611 Information Related to Geologic Time: Jurassic.

Received 19 February 2008; **Revised** 23 April 2008; **Accepted** 1 May 2008; **Published** 24 June 2008.

Jourdan, F., G. Féraud, H. Bertrand, M. K. Watkeys, and P. R. Renne (2008), The $^{40}Ar/^{39}Ar$ ages of the sill complex of the Karoo large igneous province: Implications for the Pliensbachian-Toarcian climate change, *Geochem. Geophys. Geosyst.*, *9*, Q06009, doi:10.1029/2008GC001994.

1. Introduction

[2] The Karoo large igneous province (LIP) consists of basaltic sills, dikes and lava flows that extend over more than 3×10^6 km^2 (Figure 1) [*Cox*, 1988] along with more differentiated rocks cropping out in the easternmost part of the province. It is thought to be related to the early disruption of Gondwana leading to the opening of the South Ocean. In addition, the province is synchronous with the minor Pliensbachian-Toarcian extinction and the global warming at this time [*Pálfy and Smith*, 2000].

[3] Increasing age data over the past few years [*Encarnacion et al.*, 1996; *Duncan et al.*, 1997; *Jones et al.*, 2001; *Le Gall et al.*, 2002; *Jourdan et al.*, 2004, 2005, 2007a, 2007b; *Riley et al.*, 2004, 2006] drastically improved the knowledge we have on the geodynamic history of the province. Until now, these investigations mostly focused on the lavas, dikes and sills located in Namibia, Botswana, Zimbabwe, eastern South Africa, and Lesotho. As far as geochronology is concerned, the main findings can be summarized as follows [*Jourdan et al.*, 2007b]: (1) the main volume of the basaltic sequence was emplaced over 3 to 4.5 Ma around 180 Ma whereas the entire province sustained activity over a total of 10–12 Ma (184–172 Ma), (2) brief (~1 Ma or less) and temporally (and chemically) distinct events such as the Okavango dike swarm (179.2 ± 0.4 Ma), the 800 m-thick southern Botswana lava pile (178.6 ± 0.5 Ma), the 1.9 km-thick Lesotho lava pile (181.6 ± 0.7 Ma) can be identified, (3) the basaltic magmatism was followed by a late stage silicic magmatism (from 178 to 174 Ma) and (4) the magmatic activity ended with the intrusion of the MORB-like Rooi Rand dikes [e.g., *Duncan et al.*, 1990] at 174–172 Ma, heralding the onset of the oceanization process.

[4] Yet strikingly missing from this dating effort is the huge southern sill complex cropping out in the $>0.6 \times 10^6$ km^2 Main Karoo sedimentary basin, South Africa (Figures 1 and 2) with only 3 radioisotopic ages [*Encarnacion et al.*, 1996; *Duncan et al.*, 1997; *Svensen et al.*, 2007]. Although the lava flows are generally seen as representing the main volume of the large igneous provinces, the size of the Main Karoo basin (Figure 2) along with the density of sill injection (i.e., locally representing up to 70% in volume of the basin [*Roswell and De Sward*, 1976] (Figures 2c and 2d) imply that the sill complex might actually represent a dominant expression of the magmatism in the Main Karoo basin when compared to the lava flows.

[5] So far, field relationships based on hydrothermal vent complexes related to the sill emplacements suggest that sill intrusions might, at least partially, predate the extrusion of Karoo lava flows in this area [*Ross et al.*, 2005; *Svensen et al.*, 2006a]. Other studies based on calculation of the magma driving pressure rather suggest that extrusion of the Karoo basalts began before the emplacement of the sills [*Kattenhorn and Watkeys*, 1995].

[6] Recent studies suggest that the intrusion of sills in a sedimentary basin that includes carbon and/or sulfur rich rocks might be a dominant factor responsible for climate changes through greenhouse gas emission [*Svensen et al.*, 2004, 2006b, 2007; *McElwain et al.*, 2005]. Although the Karoo LIP does not coincide with one of the *major* mass extinctions, it is synchronous with the Pliensbachian-Toarcian boundary (5% extinction of the worldwide biota), the abundant black shales reported during the Toarcian and the global warming period inferred at this time [*Bailey et al.*, 2003]. We note that *van de Schootbrugge et al.* [2005] raised the possibility that the Toarcian climate change was local and not on a planetary scale.

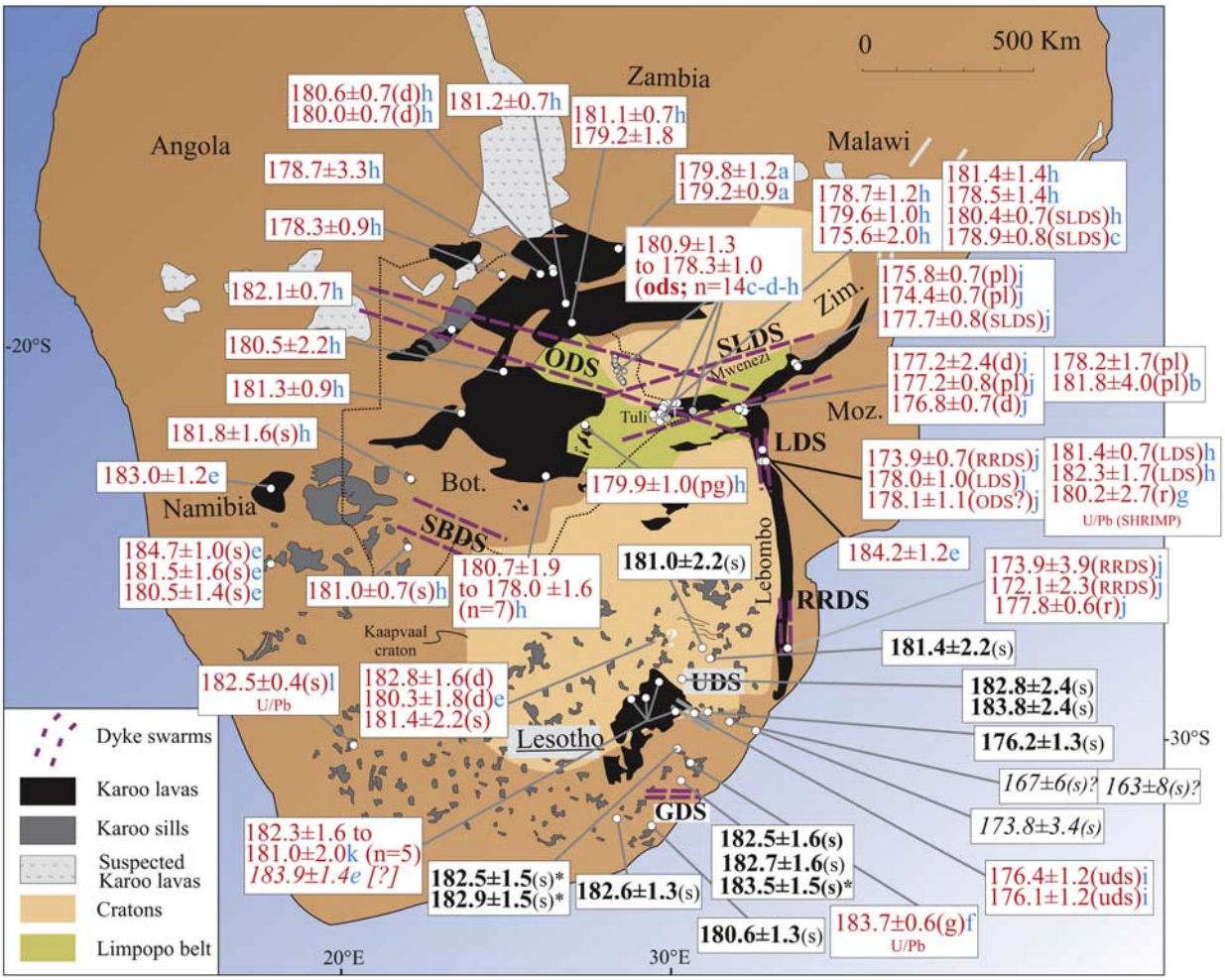

Figure 1. Sketch map of the remnants of African Karoo flood basalts, sills, and related dike swarms (modified after *Jourdan et al.* [2005]). ODS, Okavango dike swarm; SLDS, Save Limpopo dike swarm; LDS, Lebombo dike swarm; RRDS, Rooi Rand dike swarm; SBDS, south Botswana dike swarm; UDS, Underberg dike swarm; and GDS, Gap dike swarm. Previous (on mineral separates only) $^{40}Ar/^{39}Ar$ plateau and miniplateau ages and two U/Pb ages are indicated ($\pm 2\sigma$) (gray number). New $^{40}Ar/^{39}Ar$ plateau and best estimate (*) ages of the sills are indicated in bold. Three isochron ages are indicated in italic font for information, but the validity of the data is largely questionable (?; see text for discussion). Ages alone represent lava flows; otherwise, quotations in brackets beside the ages are ODS, SLDS, and LDS (corresponding dike swarm), d (dike with not well constrained direction), s (sill), pl (pluton), pg (plug), r (rhyolite), and g (granophyre).When numerous data are reported from the same locality, only bracketing ages are mentioned for clarity, with n being the number of plateau ages. Previous ages are reported as published in red with blue colored letters as follows: a, *Jones et al.* [2001]; b, *Landoll et al.* [1989]; c, *Le Gall et al.* [2002]; d, *Jourdan et al.* [2004]; e, *Duncan et al.* [1997]; f, *Encarnacion et al.* [1996]; g, *Riley et al.* [2004]; h, *Jourdan et al.* [2005]; i, *Riley et al.* [2006]; j, *Jourdan et al.* [2007a]; k, *Jourdan et al.* [2007b]; l, *Svensen et al.* [2007]. Zimb., Zimbabwe; Moz, Mozambique; Bot, Botswana.

Addressing the timing of the sill emplacement and the entire Karoo LIP is therefore crucial to investigate their roles in the Pliensbachian-Toarcian climate change.

[7] This study focuses on the sills cropping out in the eastern part of the Main Karoo basin, along a 710 km-long section (Figures 1 and 2). We present sixteen new $^{40}Ar/^{39}Ar$ analyses carried out on fresh plagioclase and biotite separates from fifteen samples. We obtained nine plateau and four miniplateau ages. These results bring important constraints for the timing of the sill complex emplacement, the

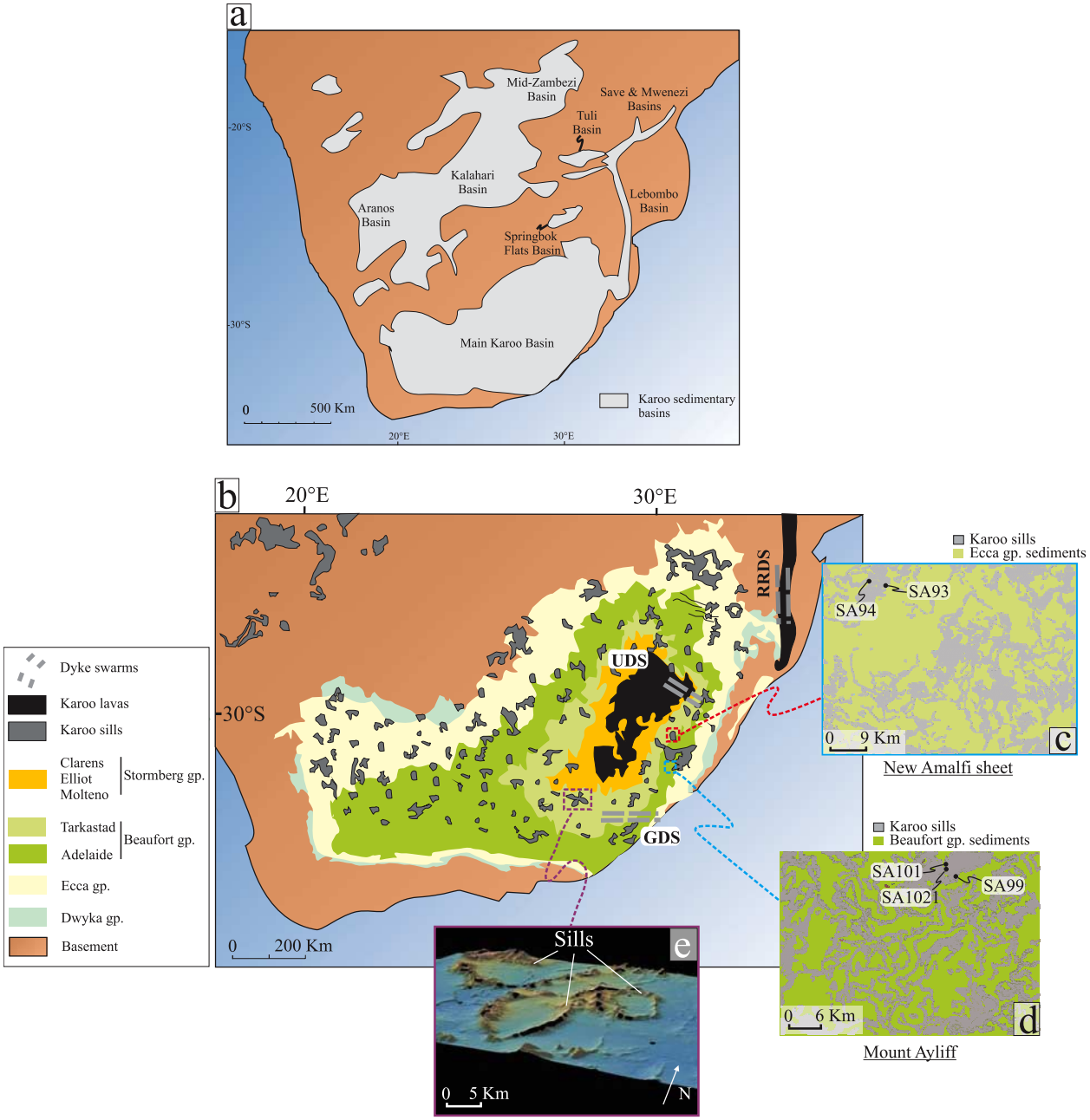

Figure 2. (a) Sketch map of southern Africa showing the major sedimentary basins. All those basins are filled with the sequence represented on Figure 3, although the thickness and volume of each layer are highly variable from basin to basin. These basins are known to be intruded by sills and dikes (Figure 1). Modified after *Catuneanu et al.* [2005]. (b) Sketch map of the Main Karoo sedimentary basin, sill intrusions, dike swarms, and lava flow covers. Sills are very partially and schematically represented; otherwise, their density would cover almost the whole sedimentary basin (see insets: Figures 2c and 2d). UDS, Underberg dike swarm; RRDS; Rooi Rand dike swarm; and GDS, Gap dike swarm. (c) New Amalfi sheet and (d) Mount Ayliff: simplified geological map of selected sampled areas showing the very large proportion of sills intruding the sediments. (e) Three-dimensional topographic map of the Golden valley area where saucer-shaped sills are exposed [see *Polteau et al.*, 2008]. The 3-D map was generated using the freeware GeomapApp available on the Web site of the Marine Geoscience Data System (http://www.marine-geo.org).

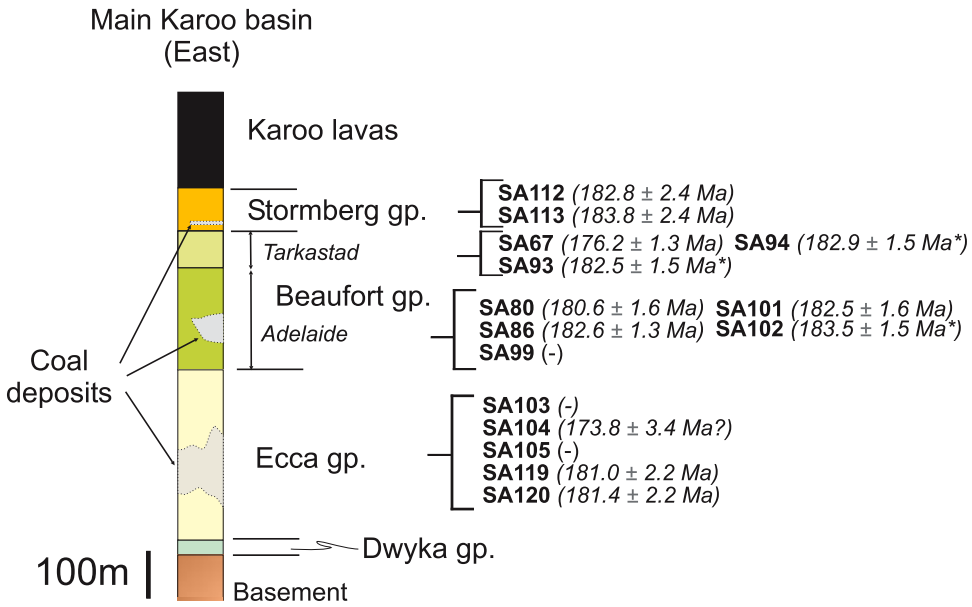

Figure 3. Synthetic stratigraphic section of the eastern portion of the Main Karoo basin. The thickness of each group is reported after *Catuneanu et al.* [2005]. Coal deposits are schematically represented in their respective sedimentary formations. Sills are not represented as their important volume and number would mask the stratigraphic sequence (see Figures 2b and 2c), but are present in the whole sequence. gp., group. Asterisk (*) indicates a high-temperature weighted-mean age preferred over the plateau age. The * ages are not reliable by themselves, but we note that they nevertheless confirm the ages obtained on other sills.

history of the entire Karoo LIP and its causal relationship with climate change.

2. Geological Background and Sample Description

2.1. Geology

[8] The Main Karoo basin (Figures 1 and 2) results from an extensive tectonic regime due to either (1) a southern subduction beneath the Panthalassan margin of Gondwana [*Catuneanu et al.*, 2005] or (2) a continental rifting heralding global continental disruption [*Turner*, 1999]. It covers more than 0.6×10^6 km^2 and comprises up to 6 km thick of clastic sediment formations capped at some places by the Karoo lava flows. The geology of the Karoo basin has been extensively described by *Catuneanu et al.* [2005] and will only be briefly summarized here. The basin mainly overlays the Paleozoic sedimentary Cape supergroup and the Namaqua-Natal Belt and consists of more than 100 Ma of sediment record. The basin includes the following from the bottom to the top (Figures 2 and 3): (1) the late Carboniferous glacial till of the Dwyka group, (2) the coal-bearing Permian marine sediments of the Ecca group (maximum thickness of 3000 m in the southern part of the basin [*Catuneanu et al.*, 2005]), (3) the Permo-Triassic fluvial sediments of the Beaufort group followed by a mid-Triassic hiatus and (4) the mid-Triassic to early Jurassic Stormberg Group. The remnant of the lava flows that may have once covered the entire Main Karoo basin consists of the up to 1900 m-thick Lesotho lava pile [e.g., *Marsh et al.*, 1997] dated at 181.6 ± 0.7 Ma [*Jourdan et al.*, 2007c]. The Main Karoo basin is heavily intruded by sills and subordinate dikes forming a vast 3-D interconnected complex throughout the entire basin [*Chevallier and Woodford*, 1999] (Figures 2b, 2c, and 2d). The intrusive rocks are more resistant to erosion compared to the sedimentary rocks and thus generally dominate the topography (Figure 2e). The sill thicknesses vary from few meters to up to 100 m. The sills reach their maximum thickness and abundance in the Beaufort group where they often display a noticeable "saucer" shape (Figure 2e) [*Chevallier and Woodford*, 1999; *Polteau et al.*, 2008]. Magmatic flow features of some sills cropping out in the eastern basin are consistent with a NNE magma flow direction [*Kattenhorn and Watkeys*, 1995]. The dikes are relatively small compared to those found in Karoo giant swarms (e.g., Okavango dike swarm [*Le Gall et al.*, 2005]) and are up to 1 m

Table 1. Summary Indicating Integrated, Plateau/Miniplateau and Isochron Ages for the Sill Plagioclase and Biotite Separates[a]

	General Characteristics					Plateau Characteristics					Isochron Characteristics						
Sample	Laboratory Number	Coordinates	Group Intruded	Mineral	Integrated Age (Ma, ±2σ)	Plateau Age/ Preferred Age* (Ma, ±2σ)	Total ^{39}Ar Released (%)	Attribute	MSWD	P	Isochron Age (Ma, ±2σ)	n	^{40}Ar/^{36}Ar Intercept (±1σ)	MSWD	P	Observation	Altitude (Meters Above Sea Level)
SA67	58224-01	29°31′26″S 29°41′18″E	Beaufort (Tarkastad)	Plg	*177 ± 1.3*	**176.2 ± 1.3**	92%	P	1.41	0.16	*176.2 ± 1.8*	13	299 ± 14	1.6	0.08	-	1840
SA80	58225-01	32°18′57″S 28°10′51″E	Beaufort (Adelaide)	Plg	*180.4 ± 1.6*	**180.6 ± 1.3**	96%	P	1.40	0.2	*181.5 ± 1.6*	12	284 ± 4	1.6	0.11	Slight ^{40}Ar loss	632
SA86	58226-01	32°30′23″S 26°48′36″E	Beaufort (Adelaide)	Plg	*182.0 ± 1.4*	**182.6 ± 1.3**	73%	P	1.30	0.23	*181.3 ± 1.4*	11	274 ± 6	1.1	0.38	Clustering near ^{39}Ar/^{40}Ar axis	1039
SA93	58227-01	30°15′13″S 29°09′11″E	Beaufort (Tarkastad)	Plg	*180.7 ± 1.6*	*179.8 ± 1.3*	68%	MP	1.69	0.10	*179.1 ± 1.6*	10	311 ± 7	1.6	0.12	-	N/A
						182.5 ± 1.5*	31%	WM	0.37	0.69							
SA94	58228-01	30°14′40″S 29°06′00″E	Beaufort (Tarkastad)	Plg	*180.8 ± 1.4*	*179.9 ± 1.3*	64%	MP	1.60	0.14	*179.9 ± 1.6*	9	308 ± 10	1.6	0.13	Clustering near ^{39}Ar/^{40}Ar axis	1586
						182.9 ± 1.5*	34%	WM	0.58	0.56							
SA99	58235-01	31°01′20″S 29°19′41″E	Beaufort (Adelaide)	Plg	*186.9 ± 3.6*	-	-	-	-	-	*176.4 ± 2.0*	12	582 ± 16	1.5	0.12	Clustering near ^{39}Ar/^{40}Ar axis	1155
SA101 (multigrains)	58236-01	31°00′15″S 29°19′09″E	Beaufort (Adelaide)	Bio	*182.6 ± 1.6*	**182.5 ± 1.6**	77%	P	0.58	0.77	*182.9 ± 1.4*	12	195 ± 7	1.0	0.45	^{39}Ar recoil redistribution	1213
SA101 (single grain)	58236-02	31°00′15″S 29°19′09″E	Beaufort (Adelaide)	Bio	*182.7 ± 1.6*	**182.7 ± 1.6**	90%	P	1.2	0.28	*182.5 ± 1.6*	14	410 ± 40	1.6	0.09	Clustering near ^{39}Ar/^{40}Ar axis	1213
SA102	58237-01	31°00′17″S 29°19′07″E	Beaufort (Adelaide)	Plg	*179.1 ± 1.2*	*179.2 ± 1.3*	49%	MP	0.8	0.55	*176.4 ± 2.6*	8	360 ± 30	1.4	0.2	Clustering near ^{39}Ar/^{40}Ar axis	?
						183.5 ± 1.5*	32%	WM	0.8	0.46							
SA103	58238-01	28°37′54″S 31°02′58″E	Ecca	Plg	*243 ± 4*		-				163 ± 8?	6	537 ± 12	1.8	0.14	-	40
SA104	58239-01	29°31′48″S 31°13′30″E	Ecca	Plg	*181.8 ± 2.0*	*173.4 ± 2.0*	54%	MP	0.5	0.59	173.8 ± 3.4?	4	459 ± 16	0.3	0.74	Four points only	0
SA105	58213-01	29°35′02″S 30°19′52″E	Ecca	Plg	*201 ± 6*	*177.3 ± 3.7*	51%	MP	1.5	0.17	167 ± 6?	11	309 ± 4	1.5	0.13	-	1057
SA112	58214-01	28°13′21″S 29°09′17″E	Stormberg	Plg	*184.1 ± 3.0*	**182.8 ± 2.4**	88%	P	0.9	0.56	*183.9 ± 3.0*	10	286 ± 9	0.8	0.63	Small spread	2113
SA113	58215-01	28°13′31″S 29°09′26″E	Stormberg	Plg	*183.6 ± 2.8*	**183.8 ± 2.4**	96%	P	0.8	0.62	*183.5 ± 3.2*	13	297 ± 17	1.6	0.08	-	1935
SA119	58216-01	26°23′41″S 28°56′13″E	Ecca	Plg	*181.4 ± 2.4*	**181.0 ± 2.2**	93%	P	0.5	0.9	*178.9 ± 2.2*	13	480 ± 40	0.4	0.96	Clustering near ^{39}Ar/^{40}Ar axis	1654
SA120	58217-01	26°27′00″S 29°26′47″E	Ecca	Plg	*181.8 ± 2.4*	**181.4 ± 2.2**	94%	P	0.5	0.85	*181.1 ± 2.2*	12	316 ± 18	1.1	0.32	Clustering near ^{39}Ar/^{40}Ar axis	1663

thick and 200 m long [*Polteau et al.*, 2008]. Only in the easternmost part of the Basin, larger dikes have been identified: (1) the Uderberg dike swarm, which yielded two plateau ages at ~176 Ma [*Riley et al.*, 2006] and thus represents a late stage activity in the history of the province, and (2) the two 100 km-long Gap dikes (Figure 1), undated yet due to significant alteration of the samples.

2.2. Sample Locations and Descriptions

[9] The fifteen investigated samples come from thirteen magmatic bodies intruding various stratigraphic levels of the Karoo supergroup (Figure 3) and located along the eastern part of the Main Karoo basin, on northeast, east and southeast of the Lesotho basalt escarpment (Figures 1 and 2). The intrusions can be subdivided into (1) the voluminous Mount Ayliff cumulate-bearing layered complex (samples SA99, SA101, SA102), intruding the Beaufort group, and (2) thinner gabbroic-doleritic sills, some of them evolving toward differentiated granophyres (New Amalfi sheet) intruding the Ecca group (samples SA103, SA104, SA105, SA119, SA120), the Beaufort group (samples SA67, SA80, SA86, SA93, SA94) and the Stormberg group (samples Sa112, SA113). Characteristics of individual sills and samples are given in Table 1.

[10] The sills samples are fine- to coarse-grained dolerites to gabbros. They show intersertal to intergranular texture and some of them (mostly to the north) display clusters of plagioclase glomerocrysts. All the sill samples contain dominantly plagioclase and augitic clinopyroxene, together with subordinate amounts of titanomagnetite and interstitial granophyric patches (from cryptocrystalline to micropegmatite associations). In addition, some samples contain variable amounts of olivine or pigeonite. The samples from the Mount Ayliff complex are mostly ultramafic to mafic cumulates, evolving from plagioclase peridotite (SA99) to olivine-gabbro (SA101) and leucogabbro (SA102). In the ultramafic rocks, the cumulus phases are olivine and spinel with intercumulus clinopyroxene, plagioclase and biotite. In the gabbroic cumulates, plagioclase becomes the dominant cumulus phase at the expense of olivine, with intercumulus clinopyroxene and orthopyroxene. The rocks are mostly fresh (LOI < 0.4 wt%), except the more altered SA67, SA103 and SA104 samples (LOI = 1.15, 0.99, 2.28 wt%, respectively). The alteration products are mainly sericite (after plagioclase), and serpentine-bowlingite (after olivine).

3. Analytical Procedures

[11] We selected fourteen fresh samples from which we separated unaltered, optically transparent plagioclase in the 200–315 μm and 125–200 μm size fraction for $^{40}Ar/^{39}Ar$ dating. In addition, one sample (SA101) was analyzed on biotite single grains and multigrains, respectively. These minerals were separated using a Frantz magnetic separator, and then carefully selected under a binocular microscope. Only absolutely transparent plagioclase grains, free of both white cracks and cloudy regions (both are potential reservoirs for sericite) were selected. Biotite was selected on the basis of the absence of inclusions and chloritization and with a large enough thickness to avoid undesirable ^{39}Ar recoil-induced loss [*Paine et al.*, 2006; *Jourdan et al.*, 2007c]. After handpicking, the plagioclase samples were further leached in diluted HF for one minute and then thoroughly rinsed with distilled water in an ultrasonic cleaner.

[12] One irradiation of 10 h duration (#346) was performed in the Cd-shielded (to minimize undesirable nuclear interference reactions) CLICIT facility of the TRIGA reactor at Oregon State University, USA. Samples were loaded into fifteen wells distributed over three stacked aluminum discs of 1.9 cm diameter and 0.3 cm depth. Hb3gr hornblende was used as neutron fluence monitor and was loaded into 7 pits per disc bracketing the samples. We calculated J values relative to an age of Hb3gr of 1072 ± 7 Ma [*Turner et al.*, 1971] and using the decay constants of *Steiger and Jager* [1977]. The 1072 Ma age for Hb3gr is equivalent to 28.03 Ma for the widely used Fish Canyon

Notes to Table 1.

[a] Plg, plagioclase; Bio, biotite. Ages in bold indicate preferred ages. Preferred ages do not necessarily represent the largest plateau section given by a sample but are based on a comparison between age and Ca/K spectra (compare to section 4). In this case, both the largest and shortest "plateau" sections are shown with the short preferred section being indicated by an asterisk (*). P, plateau; MP, miniplateau; WM, weighted mean age. We calculated J values relative to an age of Hb3gr of 1072 ± 7 Ma [*Turner et al.*, 1971] indistinguishable from the age of 1074 ± 5 Ma reported by *Jourdan et al.* [2006]. Other ages are indicated for information only. Ages in italic are considered to be not reliable (compare to section 4). Isochron ages with a "?" are statistically valid but most certainly geologically meaningless. MSWD and probability (P), percentage of ^{39}Ar degassed used in the plateau calculation, number of analyses included in the isochron, and $^{40}Ar/36Ar$ intercept are indicated. Analytical uncertainties on the ages are quoted at 2 sigma (2σ) confidence levels and at 1σ for the $^{40}Ar/^{36}Ar$ intercept.

sanidine standard [*Renne et al.*, 1998] based on the intercalibrations of *Jourdan et al.* [2006] and *Jourdan and Renne* [2007] and is indistinguishable from the age of 1074 ± 5 Ma reported by *Jourdan et al.* [2006].

[13] The mean J values for each of the three discs are 0.002656 ± 0.000009 (0.34%), 0.002659 ± 0.000011 (0.43%) and 0.002620 ± 0.000015 (0.58%), each determined as the arithmetic mean of J values for 7 wells of the irradiation disc interspersed with the samples. The correction factors for interfering isotopes correspond to the weighted mean of 10 years of measurements of K-Fe and $CaSi_2$ glasses and CaF_2 fluorite in the OSTR reactor: $(^{39}Ar/^{37}Ar)_{Ca} = (7.60 \pm 0.09) \times 10^{-4}$; $(^{36}Ar/^{37}Ar)_{Ca} = (2.70 \pm 0.02) \times 10^{-4}$; and $(^{40}Ar/^{39}Ar)_{K} = (7.30 \pm 0.90) \times 10^{-4}$.

[14] Analyses of $^{40}Ar/^{39}Ar$ were performed at the Berkeley Geochronology Center. The multigrain samples were degassed using a CO_2 laser focused with a beam-integrator lens and the single biotite sample using a focusing lens. The gas was purified in a stainless steel extraction line using two C-50 getters and a cryogenic condensation trap. Ar isotopes were measured in static mode using a MAP 215–50 mass spectrometer with a Balzers electron multiplier mostly using 10 cycles of peak-hopping. A more complete description of the mass spectrometer and extraction line is given by *Renne et al.* [1998]. Blank measurements were generally obtained before and after every three sample runs. Mass discrimination, assuming a power law relationship between D and atomic mass, was monitored several times a day (every 9 steps) and provided mean values of 1.00564 ± 0.00182 per dalton (atomic mass unit). Ar isotopic data corrected for blank, mass discrimination and radioactive decay are given in auxiliary material Data Set S1. Individual errors in Data Set S1 are given at the 1σ level. Our criteria for the determination of plateau and miniplateau ages are as follows: plateaus must include at least 70% of ^{39}Ar released and miniplateau between 50 and 70%. They should be both distributed over a minimum of 3 consecutive steps agreeing at 95% confidence level and satisfying a probability of fit of at least 0.1. Plateau ages are given at the 2σ level and are calculated using the mean of all the plateau steps, each weighted by the inverse variance of their individual analytical error. Integrated ages (2σ) are calculated using the total gas released for each Ar isotope. Inverse isochrons include the maximum number of consecutive steps with a probability of fit $\geq$0.05. The uncertainties on the $^{40}Ar^*/^{39}Ar$ ratios of the monitors are included in the calculation of the integrated and plateau age uncertainties, but not the errors on the age of the monitor and on the decay constant (internal errors only; see discussion by *Min et al.* [2000]). Detailed $^{40}Ar/^{39}Ar$ results are shown in auxiliary material Data Set S1[1] and are summarized in Table 1.

4. The $^{40}Ar/^{39}Ar$ Results

[15] We obtained nine plateau and four miniplateau ages (including one duplicate) ranging from 176.2 ± 1.3 to 183.8 ± 1.4 Ma and with MSWD ranging from 0.46 to 1.6 and probability ranging from 0.1 to 0.9 (Figure 4; in bold in Table 1). The age spectra show generally some disturbances on the first ~5–10% of ^{39}Ar degassed before meeting the plateau criteria. The single-grain (182.7 ± 1.6 Ma) and multigrain (182.5 ± 1.6 Ma) biotite duplicate of sample SA101 show a perfect age agreement. Although classical recoil redistribution seems to affect slightly the low-temperature section of the biotite age spectra, the total gas ages are virtually identical to the plateau ages, thus attesting of the validity of these ages [*Nomade et al.*, 2004]. We use hereafter an age of 182.6 ± 1.6 Ma for SA101 corresponding to the arithmetic mean between the single-grain and multigrain analyses. Plagioclase separates from samples SA67, SA80, SA86, SA112, SA113, SA119 and SA120 yield flat and well-behaved plateau ages.

[16] One sample (SA102) shows a continuously increasing age spectrum with a flat midsection. The intermediate steps almost meet our criteria of a miniplateau age at 179.2 ± 1.3 Ma over 49% of the ^{39}Ar released (MSWD = 0.83; P = 0.55). However, this spectrum shows the usual characteristics of $^{40}Ar^*$ loss with individual steps that gradually tend to converge toward a minimum age over the last steps. The three last steps (not included in the miniplateau) show an older weighted mean age of 183.5 ± 1.5 Ma that might represent the closest estimates of the emplacement age. Sample SA99 failed to yield a miniplateau and gave a weighted mean age of 183.8 ± 2.0 Ma over 58% of the age spectrum. Although ages obtained for SA99 and SA102 do not meet the definition of a plateau and should not be included in the Karoo age database, we note that their ages (high-temperature age for

[1] Auxiliary materials are available at ftp://ftp.agu.org/apend/gc/2008gc001994.

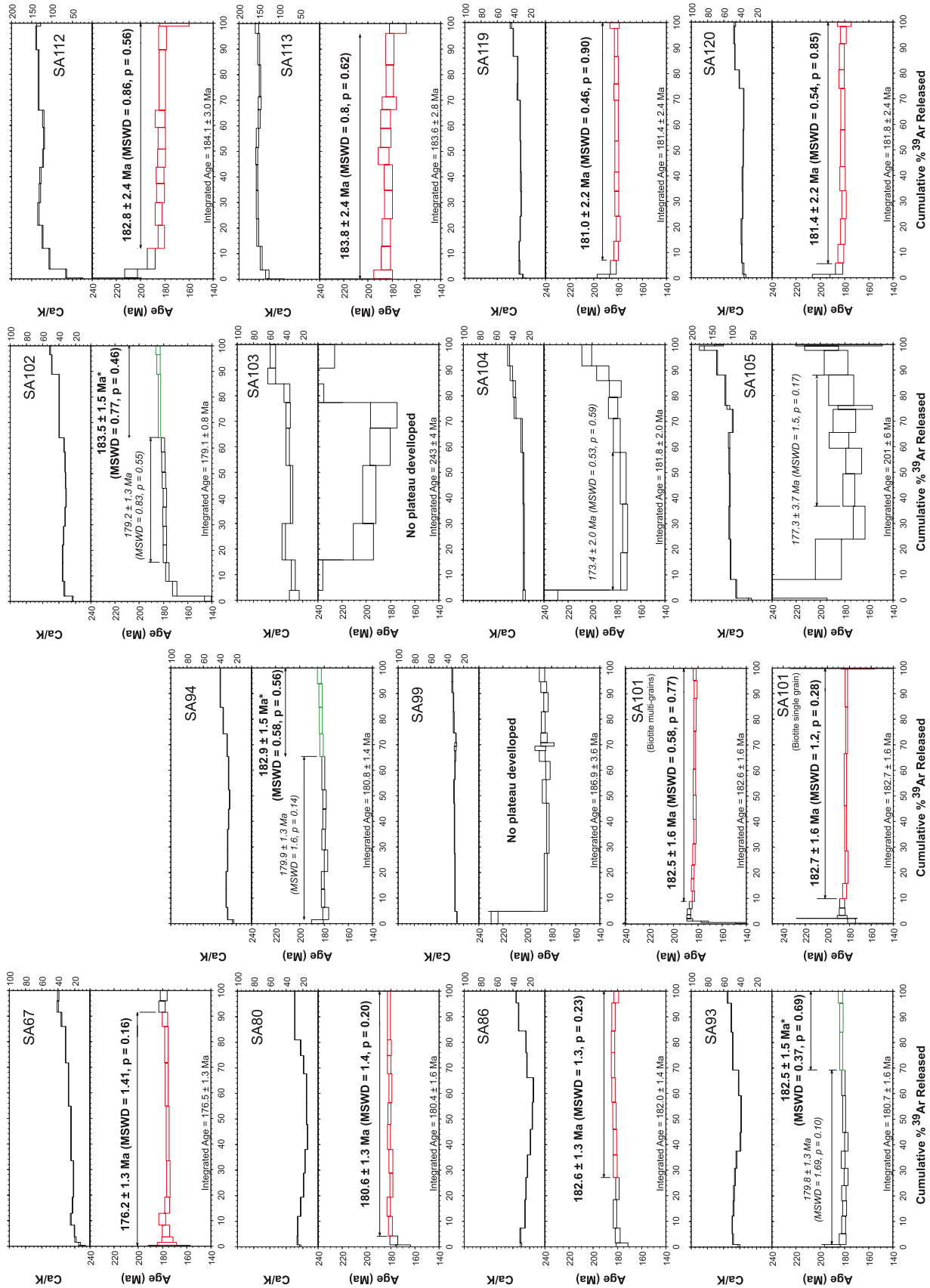
SA112
182.8 ± 2.4 Ma (MSWD = 0.86, p = 0.56)
Integrated Age = 184.1 ± 3.0 Ma
SA113
183.8 ± 2.4 Ma (MSWD = 0.8, p = 0.62)
Integrated Age = 183.6 ± 2.8 Ma
SA119
181.0 ± 2.2 Ma (MSWD = 0.46, p = 0.90)
Integrated Age = 181.4 ± 2.4 Ma
SA120
181.4 ± 2.2 Ma (MSWD = 0.54, p = 0.85)
Integrated Age = 181.8 ± 2.4 Ma
SA102
183.5 ± 1.5 Ma*
(MSWD = 0.77, p = 0.46)
179.2 ± 1.3 Ma
(MSWD = 0.83, p = 0.55)
Integrated Age = 179.1 ± 0.8 Ma
SA103
No plateau develloped
Integrated Age = 243 ± 4 Ma
SA104
173.4 ± 2.0 Ma (MSWD = 0.53, p = 0.59)
Integrated Age = 181.8 ± 2.0 Ma
SA105
177.3 ± 3.7 Ma (MSWD = 1.5, p = 0.17)
Integrated Age = 201 ± 6 Ma
SA94
182.9 ± 1.5 Ma*
(MSWD = 0.58, p = 0.56)
179.9 ± 1.3 Ma
(MSWD = 1.6, p = 0.14)
Integrated Age = 180.8 ± 1.4 Ma
SA99
No plateau develloped
Integrated Age = 186.9 ± 3.6 Ma
SA101
(Biotite multi-grains)
182.5 ± 1.6 Ma (MSWD = 0.58, p = 0.77)
Integrated Age = 182.6 ± 1.6 Ma
SA101
(Biotite single grain)
182.7 ± 1.6 Ma (MSWD = 1.2, p = 0.28)
Integrated Age = 182.7 ± 1.6 Ma
SA67
176.2 ± 1.3 Ma (MSWD = 1.41, p = 0.16)
Integrated Age = 176.5 ± 1.3 Ma
SA80
180.6 ± 1.3 Ma (MSWD = 1.4, p = 0.20)
Integrated Age = 180.4 ± 1.6 Ma
SA86
182.6 ± 1.3 Ma (MSWD = 1.3, p = 0.23)
Integrated Age = 182.0 ± 1.4 Ma
SA93
182.5 ± 1.5 Ma*
(MSWD = 0.37, p = 0.69)
179.8 ± 1.3 Ma
(MSWD = 1.69, p = 0.10)
Integrated Age = 180.7 ± 1.6 Ma
Ca/K
Age (Ma)
Cumulative % ^{39}Ar Released

Figure 4

SA102) are in good agreement within uncertainties with the age of the cogenetic rock SA101, sampled from the same Mount Ayliff complex (Figure 2d).

[17] SA93 and SA94 show two statistically robust miniplateau ages at 179.8 ± 1.3 Ma (MSWD = 1.69; P = 0.10) and 179.9 ± 1.3 Ma (MSWD = 1.60; P = 0.14). However, a closer inspection to their Ca/K and ages spectra shows that Ca/K and age co-vary, both of them following a slight but noticeable tilde-shape pattern. This behavior may be interpreted as reflecting sericite alteration after plagioclase, which tends to bias the ages toward younger values [e.g., *Verati and Féraud*, 2003; *Fuentes et al.*, 2005]. The sericite tends to degas in a narrow intermediate temperature range and causes the depression in the Ca/K and age patterns. In this case, ages obtained from higher Ca/K portion of the spectra (i.e., here from higher temperature steps) are closer minimum estimate of the crystallization age [*Jourdan et al.*, 2004]. An alternative interpretation is that the tilde-shaped Ca/K and age spectra reflect the effects of cryptic antiperthite exsolution combined with ^{39}Ar and ^{37}Ar recoil effects [e.g., *De Min et al.*, 2002; *Rosset et al.*, 2007], which in some cases permits no reliable age determination. For both samples, the three and four highest temperature steps yield minimum ages of 182.5 ± 1.5 Ma (SA94; MSWD = 0.37; P = 0.69; 31% of ^{39}Ar) and 182.9 ± 1.5 Ma (MSWD = 0.58; P = 0.56; 34% of ^{39}Ar), respectively. These 2 dates are still statistically indistinguishable from each other and we tentatively conclude that they represent a better estimate of the crystallization ages of SA93 and SA94.

[18] In the inverse isochron diagram, all these samples yielded poorly defined initial $^{40}Ar/^{36}Ar$ values (Table 1) due to a strong clustering of the data near the $^{39}Ar/^{40}Ar$ axis. This prevents the determination of statistically meaningful isochron ages and $^{40}Ar/^{36}Ar$ intercepts for these samples.

[19] Three sills sampled in close proximity to each other (SA103, SA104 and SA105; Figure 1 and Table 1) failed to yield plateau ages (but 2 yield miniplateau ages). However, they show classical saddle shaped age spectra usually indicating incorporation of excess $^{40}Ar^*$ (Figure 4) [e.g., *Kelley*, 2002]. When homogeneous excess $^{40}Ar^*$ is trapped in a sample and the total ^{40}Ar represent an homogeneous mixing between the excess $^{40}Ar^*$ and the radiogenic $^{40}Ar^*$ produced after the crystallization of the samples, isochrons have been proven a useful technique to obtain meaningful ages [*Merrihue and Turner*, 1966; *Roddick*, 1978; *Heizler and Harrison*, 1988; *Renne et al.*, 1997; *Sharp and Renne*, 2005]. The three samples yield isochron ages ranging from 163 ± 8 Ma to 173.8 ± 3.4 Ma (Figure 5). The $^{40}Ar/^{36}Ar$ intercepts confirm that these samples include nonatmospheric initial ratios with value ranging from 309 ± 4 to 537 ± 12. They yield MSWD values ranging from 0.3 to 1.8 and probabilities of 0.13 to 0.74. The isochron from sample SA104 is, however, based only on four unevenly distributed steps but the ''bottom'' of the saddle spectra of sample yielded a miniplateau age at 173.4 ± 2.0 Ma (Figure 4 and Table 1) indistinguishable from the isochron age. Nevertheless, these ages will not be considered further in the next discussion due to their extremely poor reliability along with possible alteration.

[20] The Ca/K mean ratio values of the plagioclase samples range from ~30 to ~150 (Figure 4 and auxiliary material Data Set S1). Ca/K spectra shapes range from flat to slightly tilde (~) shaped. The tilde shape is interpreted in term of alteration signature when co-varying with ages [e.g., *Verati and Féraud*, 2003; *Fuentes et al.*, 2005], as observed for samples SA93 and SA94 and as mentioned above. We note that tilde-shaped Ca/K profiles are observed for some other samples (e.g., SA80, SA86) but that no correlation with age is observed. In this case, the tilde-shaped pattern might be caused by (1) plagioclase compositional zoning, (2) alkali feldspar subsolidus exsolution or (3) essentially syn-eruptive alteration (F. Jourdan, unpublished data, 2007). The latter explanation is favored here, as the two former features are not observed in thin section contrary to minor sericite in plagioclase cracks. Yet in the

Figure 4. The $^{40}Ar/^{39}Ar$ apparent age and related Ca/K ratio spectra of the plagioclase separates versus the cumulative percentage of ^{39}Ar released. Steps included in the plateau (>70% ^{39}Ar released) and miniplateau (50–70% ^{39}Ar released) age calculation are indicated in red. Errors on plateau and miniplateau ages are quoted at 2σ and do not include systematic errors (i.e., uncertainties on the age of the monitor and on the decay constant). MSWD and probability are indicated. Ages in bold represent the most reliable ages for each sample. An asterisk (*) indicates a high-temperature weighted-mean age (green steps) preferred over the plateau age.

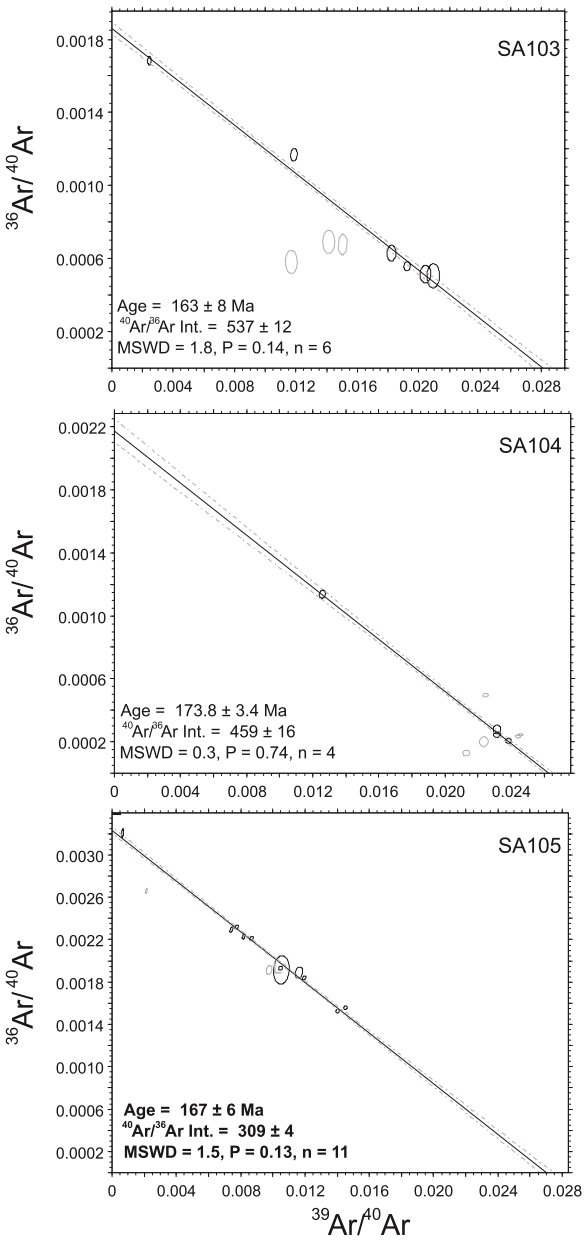

Figure 5. Inverse correlation isochron plot of $^{36}Ar/^{40}Ar$ versus $^{39}Ar/^{40}Ar$ for three step-heated samples (SA103, SA104, and SA105) that have incorporated $^{40}Ar^*$ in excess. MSWD and probability, and $^{40}Ar/^{36}Ar$ intercept are indicated. We set a probability filter of 0.05 as a probability cutoff to eliminate steps. Excluded steps are indicated in gray.

three cases, the $^{40}Ar/^{39}Ar$ age reflects the age of plagioclase crystallization within error.

[21] Two samples (SA112, SA113) show high Ca/K ratio (>140) which tends to lower the precision on the plateau ages because of the more important corrections for Ca-induced interferences and the smaller ^{39}Ar ion beams.

5. Discussion

5.1. Sill Complex in the Karoo Large Igneous Province

5.1.1. Age and Duration of the Eastern Sill Complex and Karoo Province

[22] Previous estimates of the duration of the sill emplacement (although based on a single age each) quoted an interval of less than 1 Ma [*Encarnacion et al.*, 1996; *Svensen et al.*, 2007] similar to the duration previously referenced for the total duration of the province [*Duncan et al.*, 1997]. The new results obtained on the sills from the eastern Main Karoo basin show a relatively large range of plateau and miniplateau ages (176.2 ± 1.3 to 183.8 ± 2.4 Ma; Table 1) suggesting that the sills have not been emplaced in a brief magmatic event but rather through a more sustained magmatic activity. Although more data are required, we suggest this duration is likely to be extrapolable to the Main Karoo basin. No apparent relationship between the emplacement depth of the sills or the sedimentary formation that they intruded and their ages are observed (Figure 3). To shed some light on the emplacement sequence of the sills, we plot the plateau and miniplateau ages in a combined probability density distribution (PDD) histogram plot (Figure 6a) [*Sircombe*, 2004]. This graph considers both the error on the individual measurement (PDD) and the number of data (histogram) responsible for a given probability peak. It has the potential to show eventual age cluster(s). In our case, the whole data define a large concentration of ages between 181 and 184 Ma, suggesting a probable duration of the main sill activity of ~3 Ma. This cluster of ages define two age populations in the histogram (Figure 6a) at ~181 Ma and 183 Ma although it is not clear whether they represent two geological events or are rather statistical artifacts due to sampling bias due to the still relatively low number of data (11 dates in the main peak). Moreover, one sample at 176.2 Ma indicates a late period of magmatism. The investigated eastern sill complex thus seems to present a microcosm of the entire Karoo igneous province, i.e., several episodic events each possibly lasting a few million years, the sum total of which spans several million years.

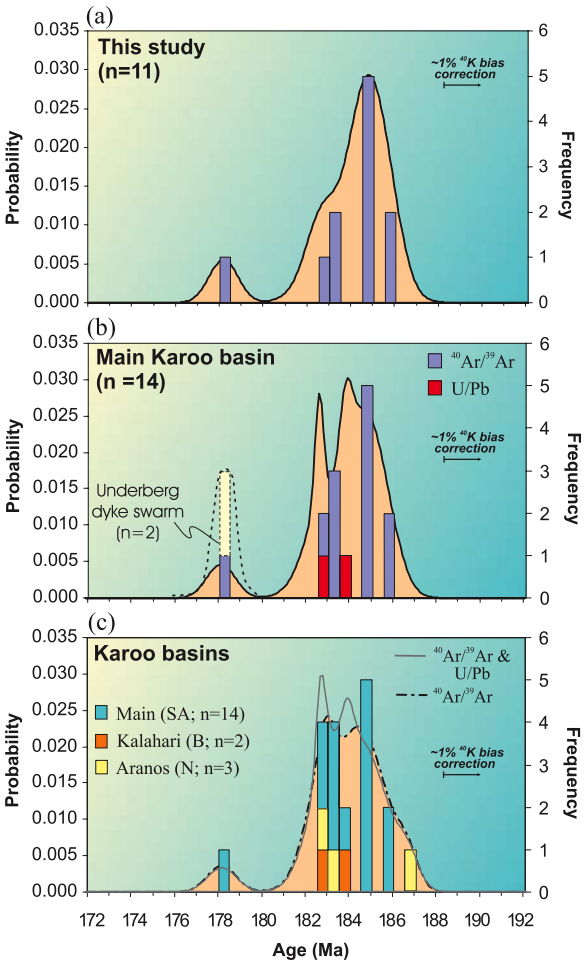

Figure 6. Age frequency histogram (error bars not included) and probability density distribution diagram (PDD; error bars included in the curve calculation) for the Karoo sills. All ages have been corrected for the ~1% bias of the ^{40}K decay constant using the decay constant proposed by *Mundil et al.* [2006]. (a) Eleven ages on sills (including two plateau-age duplicates of SA101 merged into a single age) that yielded $^{40}Ar/^{39}Ar$ plateau and best estimates ages. (b) Same as Figure 6a plus 2 U/Pb ages [*Encarnacion et al.*, 1996; *Svensen et al.*, 2007] and 1 $^{40}Ar/^{39}Ar$ age by *Duncan et al.* [1997] (compare to Figure 1). Two ages from the Underberg dike swarm are shown for comparison [*Riley et al.*, 2006]. (c) The $^{40}Ar/^{39}Ar$ (16 analyses [*Duncan et al.*, 1997; *Jourdan et al.*, 2005; this study]) and U/Pb (2 analyses [*Encarnacion et al.*, 1996; *Svensen et al.*, 2007]) for sills intruding three Karoo sedimentary basins (SA, South Africa; B, Botswana; N, Namibia; compare to Figures 1 and 7). PDD curves calculated using *Sircombe* [2004]. Dashed line represents the probability curves if the two Underberg dikes are taken into account in the PDD calculation. Note that in Figures 6b and 6c the PDD curves are strongly dependent on the two U/Pb ages due to their lower uncertainties. In this case, the peaks formed by the PDD curves are most likely a statistical artifact.

[23] The sill yielding the youngest plateau age at 176.2 ± 1.3 Ma (SA67) is close to the Underberg dike swarm (Figure 1) from which two reliable plateau ages 176.4 ± 1.2 Ma and 176.1 ± 1.2 Ma have been obtained [*Riley et al.*, 2006] (Figure 6b). These authors reported a third miniplateau age at 181.7 ± 0.7 Ma, but this age is based on three steps from a discordant spectrum possibly affected by alteration combined with excess Ar and would require confirmation. Therefore, a late ~176 Ma magmatic event formed a "hot line" that extended southeastward from the formerly emplaced Lesotho basalt (~182 Ma [*Jourdan et al.*, 2007b]) toward the future continental margin (current SE African coast). This hot line is parallel to the Underberg dike swarm and at high angle to the rifted margin. These samples are not located along the Lebombo, but they are still fairly close to the east African continental margin. Strong extension associated with the continental breakup that occurred at that time near the future rift locus might have facilitated the ascent of the magma by decompression melting, as proposed for the Karoo silicic and MORB like late magmatic activity [*Jourdan et al.*, 2007a]. We note that 3 additional samples (SA103, SA104, SA105) that yielded relatively young isochron ages at 163 ± 8 Ma, 167 ± 6 Ma and 173.8 ± 3.4 Ma, are also located on this young "hot line." However, their extremely poor reliability along with excess $^{40}Ar^*$ and possible alteration strongly question the significance of these ages.

[24] The relatively long emplacement duration observed for the sills is unlikely to represent inconsistency of the $^{40}Ar/^{39}Ar$ analyses because (1) the analyzed samples are from a single irradiation and J values have been calculated using the same reliable Hb3gr standard [*Jourdan et al.*, 2006], (2) previous $^{40}Ar/^{39}Ar$ analyses on mineral separates (mainly plagioclase) have been proven to be an extremely efficient way to identify brief events (≤1 Ma) when a statistically significant number of samples is measured (i.e., the southern Botswana lava pile, n = 7; the Okavango dike swarm, n = 14 and the Lesotho sequence, n = 5 [*Jourdan et al.*, 2005, 2007b]), (3) samples from sills in close proximity to each other yield indistinguishable ages (e.g., SA119–SA120, SA112–SA113, SA93–SA94 (and possibly SA99 to SA102 if we include the weighted mean ages; Figure 2 and Table 1)) and (4) this duration is in agreement with a relatively long duration of the main basaltic activity of the whole Karoo province (i.e., 4 ± 1 Ma [*Jourdan et al.*, 2007b]).

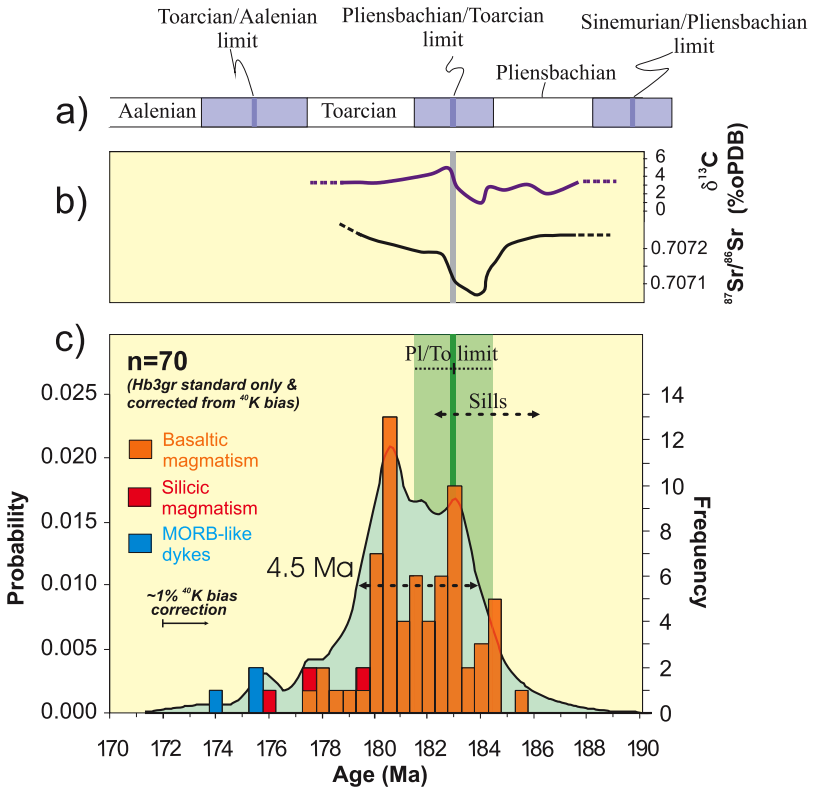

Figure 7. (a) Chronostratigraphic timescale. Stage boundary ages include U/Pb dates and their respective uncertainties (modified from *Gradstein et al.* [2004]; see text for discussion). (b) Synthetic Sr and C isotope curves based on the data of *Bailey et al.* [2003]. The Pliensbachian-Toarcian boundary is indicated. Note that the stratigraphic position of the boundary relative to the isotope record is not dependent on any radiometric ages. (c) The ^{40}K bias corrected $^{40}Ar/^{39}Ar$ age probability density distribution diagram (PDD) and frequency histogram (error bars not included) of 70 rocks of the Karoo province. We used $^{40}Ar/^{39}Ar$ ages that have been obtained using the Hb3gr standard only [*Le Gall et al.*, 2002; *Jourdan et al.*, 2004, 2005, 2007a, 2007b], to avoid results obtained with poorly calibrated standards. The age duration of the sills is indicated. The PDD curve suggests a duration of 4 ± 1 Ma (at the midheight of the peak) for the main pulses of the magmatism and 8–10 Ma for the entire Karoo province.

[25] To better refine the total duration of the Karoo province, we add the new ages obtained in this study to the existing Karoo age database (Figure 1 and associated references). However, as we did previously [*Jourdan et al.*, 2007b], we choose to plot plateau and miniplateau ages determined using homogeneous and fully calibrated standards [e.g., *Jourdan and Renne*, 2007] only. In the case of the Karoo database, this includes only ages measured with the standard Hb3gr. Results are plotted in Figure 7c. Altogether, previous and new results confirm a long lasting activity for the main volume of the province of 4 ± 1 Ma (Figure 7c), in contrast to other CFBs emplaced in 1 Ma or less (e.g., Deccan and Siberia Traps [*Hofmann et al.*, 2000; *Reichow et al.*, 2002; *Courtillot and Renne*, 2003; *Gérard et al.*, 2006]). This also shows that the first basaltic activity did not start at a specific location of the province but rather at several distinct locations in southern Africa, though a general shift of activity from south-southwest (184–181 Ma) to north (182–178 Ma) is observed (Figure 1) [e.g., *Jourdan et al.*, 2005, 2007b].

5.1.2. The $^{40}Ar/^{39}Ar$ and U/Pb Ages of the Sill Complex From the Main Karoo Basin

[26] *Encarnacion et al.* [1996] reported a U/Pb age of 183.7 ± 0.6 Ma for a granophyre from the New Amalfi sheet, east of the Lesotho basalt in South Africa (Figures 1 and 2). The U/Pb age was obtained on two 40–100 μm zircon multigrain aliquots and a concordant baddeleyite multigrain aliquot. More recently, *Svensen et al.* [2007] obtained a U/Pb age on single abraded zircon grains at 182.5 ± 0.4 Ma on a differentiated pegmatite from a sill emplaced at the westernmost extremity of the basin.

[27] Although these 2 ages are largely concordant with some of the oldest ages we obtained from the eastern Main Karoo basin sills (e.g., SA113), it

should be kept in mind that, according to recent comparative studies between $^{40}Ar/^{39}Ar$ and U/Pb ages [*Min et al.*, 2000; *Kwon et al.*, 2002; *Mundil et al.*, 2006] the value of ^{40}K decay constant is likely to be miscalibrated by ~1%, in particular the electron capture decay branch. As a consequence, ages determined by K/Ar (and $^{40}Ar/^{39}Ar$) are likely to be 1%-shifted toward younger values in Phanerozoic time compared with U-Pb ages [*Mundil et al.*, 2006].

[28] When we apply a +1% correction to the $^{40}Ar/^{39}Ar$ ages, as based on decay constants and standard calibration of *Mundil et al.* [2006], the two available U/Pb ages on the sills fall near the younger end of the main group of $^{40}Ar/^{39}Ar$ dates (i.e., 183–186 Ma) that we obtained for sills of the eastern Karoo basin (Figure 6b). Samples SA93 and SA94 both come from doleritic parts of the New Amalfi sill as well. The two (bias corrected) plateau ages at ~182 Ma might be compromised by some alteration as monitored by the Ca/K covarying ratios. However, the high temperature-step weighted-mean (+1% bias corrected) ages give minimum emplacement ages (i.e., minimum contribution of $^{40}Ar/^{39}Ar$ by sericite) at 184.3 ± 1.5 Ma (SA93) and 184.7 ± 1.5 Ma (SA94). Those two ages are statistically indistinguishable from the age obtained by *Encarnacion et al.* [1996] at 183.7 ± 0.6 Ma. Figure 6b shows two sharp probability peaks slightly offset from the histogram sample distribution, but this seems to be a statistical artifact due to the higher precision of the 2 U/Pb ages over the 12 $^{40}Ar/^{39}Ar$ ages. These PDD peaks are therefore geologically meaningless.

[29] We do not have any date on the western sills, yet the age of *Svensen et al.* [2007] falls within the range of the (corrected) ages we obtained on the eastern sills. *Svensen et al.* [2007] use this *single* age to estimate the duration of the sills to less than 1 Ma. However, all the data available on the sill complex from the Main Karoo basin plotted together (Figure 6b) do not corroborate their interpretation. The 14 ages rather suggest an emplacement duration of ~3 Ma (i.e., from 186 to 183 Ma) and even a second pulse few million years later at 178 Ma (Figure 6b). This duration is corroborated by sill age data from other basins (Figure 6c).

5.2. Pliensbachian-Toarcian Extinction and the Toarcian Oceanic Anoxic Event

5.2.1. Pliensbachian-Toarcian Boundary

[30] Large igneous provinces have been proposed to be associated with the dramatic mass extinctions that punctuate the earth history [e.g., *Courtillot and Renne*, 2003; *Wignall*, 2005]. Although the ultimate causes that trigger mass extinction and drastic climate change are difficult to assess, huge outpouring of SO_2, NO_x, halogens (F and Cl) and CO_2 may have a substantial impact on the ecosystem both directly and through various feedback mechanisms (e.g., release of methane hydrates [*Beerling and Berner*, 2002]) and over variable timescales.

[31] The Karoo LIP, despite being one of the largest CFB, is not associated with one of the 5 *major* mass extinctions. It is nevertheless possibly associated with the minor Pliensbachian-Toarcian boundary (183.0 ± 1.5 Ma [*Pálfy and Smith*, 2000; *Gradstein et al.*, 2004]). This is a second-order crisis that affected "only" ~5% of the worldwide families [*Little and Benton*, 1995]. The boundary is broadly synchronous with negative $^{87}Sr/^{86}Sr$ and negative then positive $\delta^{13}C$ seawater excursions and inferred global warming [*Little and Benton*, 1995; *Wignall*, 2001; *Bailey et al.*, 2003] (Figures 7a and 7b). The possibility that isotopic excursions are not a global phenomena has been raised by *van de Schootbrugge et al.* [2005], but many results seem to suggest that the phenomenon occurs on a planetary scale [*McElwain et al.*, 2005]. Conventional explanations for the Sr isotopic excursion often cite the weathering of the recently emplaced flood basalts and the subsequent influx of mantle-dominated (i.e., low $^{87}Sr/^{86}Sr$) Sr into the ocean. The negative $\delta^{13}C$ excursion is attributed to biogenic carbon input in the ocean (e.g., methane hydrate release or continental vegetation draining) whereas the positive excursion is likely to reflect the atmospheric and oceanic CO_2 saturation or productivity shut down [*Wignall*, 2005]. The seawater isotopic record coupled with the high concentration of black shales during most of the Toarcian both suggest protracted global anoxia conditions during this stage.

5.2.2. Age of the Pliensbachian-Toarcian Boundary Compared to the Karoo Province

[32] The $^{40}Ar/^{39}Ar$ age database is now sufficiently large to *confidently* compare the age and duration of the Karoo province with the age of the Pliensbachian-Toarcian boundary and associated isotopic shifts. The age of the Pliensbachian-Toarcian boundary has been determined using zircon U/Pb data [*Pálfy and Smith*, 2000; see also *Gradstein et al.*, 2004] and is therefore not directly comparable to the $^{40}Ar/^{39}Ar$ ages due to miscalibration problem of the ^{40}K decay constant (see discussion

above). We have shifted the entire $^{40}Ar/^{39}Ar$ histogram and PDD curve in Figure 7c by +1% (see discussion above) to allow a direct comparison between the Karoo province and the Pliensbachian-Toarcian boundary. This procedure allows all the data to be calibrated relative to the stratigraphic timescale [*Gradstein et al.*, 2004].

[33] The boundary and isotope excursions coincide with the onset of the main Karoo activity (i.e., the first large probability peak). A closer inspection shows that this period corresponds to the emplacement of the sills in the sediments of the Karoo basins and to an apparent increase in magma emplacement rate occurring only slightly after the very onset of the magmatism (Figure 7c). The large uncertainty on the age of the Pliensbachian-Toarcian boundary and the remaining uncertainty in the ^{40}K decay constant preclude more detailed comparison with the Karoo LIP, but Figure 7c strongly suggests that the isotope shifts occur *after* the onset of the Karoo magmatism and are a direct consequence of the increase of the magmatic activity and the intrusion of sills into C-rich layers. The extinction certainly characterizes well the Pliensbachian-Toarcian boundary but species-level extinctions continued 3–4 million years after the boundary perhaps in association with the reported oceanic anoxic event [*Pálfy and Smith*, 2000]. This was synchronous with, and may have been related to the protracted magmatic activity, although the magma emission substantially decreased ~4 Ma after the onset of activity (Figure 7c).

[34] At that point two outstanding questions arise: (1) what are the exact causes for the $\delta^{13}C$ shifts and global warming, and (2) why did the Karoo LIP not trigger a more significant mass extinction despite its large size?

5.2.3. Role of Volcanic Eruptions and Sill Injections in Climate Change?

[35] As previously told, the Pliensbachian-Toarcian extinction coincides with shifts in the $\delta^{13}C$ and $^{87}Sr/^{86}Sr$ isotope records, oceanic anoxia and short global warming. Isotopic shifts occurred during the onset of the major activity of the Karoo province (Figure 7).

[36] CO_2 release from the Karoo basalts alone has been suggested to be insufficient to explain the isotopic shifts and inferred major climate change at this time [*Self et al.*, 2005; *Beerling and Brentnall*, 2007]. However, this interpretation is based on a volcanogenic $\delta^{13}C$ value of −6‰. *Suan et al.* [2008] argued that the range of reported $\delta^{13}C$ values of mantle xenoliths suggest a bimodal distribution of −6‰ and −25‰ [*Deines*, 2002] and that a mean $\delta^{13}C$ value of −23‰ have been reported for some flood basalts [*Hansen*, 2006]. In the case of a $\delta^{13}C$ value of −25‰ for mantle carbon, only ~7000 Gt of volcanogenic carbon would be necessary to explain the $\delta^{13}C$ shift measured at the Pliensbachian-Toarcian boundary [*Suan et al.*, 2008]. This value is a compatible with minimum volume estimates of volcanogenic CO_2 emitted by the Karoo province (~9000 Gt C [*Beerling and Brentnall*, 2007]). In addition, it has been recently proposed by *Self et al.* [2006] that repeated volcanogenic SO_2 injections may have triggered severe climatic perturbations as well.

[37] As said previously, a sudden increase of the Karoo magma eruption rate (and thus CO_2 and SO_2 release) coincides within uncertainties with the Pliensbachian-Toarcian boundary and associated isotopic shifts and inferred climate change. However, if the main volume of the Karoo magma has been emitted in several pulses over several million years [*Jourdan et al.*, 2005, 2007b], and not during a $\ll$ 1 Ma long event, then additional phenomena are required to explain the climate perturbations, in particular the 0.9 Ma total duration [*Suan et al.*, 2008] of the $\delta^{13}C$ excursion.

[38] Two others possible culprits that could have acted in conjunction with the volcanogenic CO_2 emission are the CH_4 released from gas hydrate reservoir buried in seafloor sediments [e.g., *Wignall*, 2005, and references therein] and CH_4 and CO_2 released in response to the intrusion of magma in sedimentary carbon rich layers [*Svensen et al.*, 2004, 2007]. Evidence for methane release from marine sediments is somewhat hard to find in geological records and only indirect clues are available (e.g., $\delta^{13}C$ negative shift), but it could represent as much as 5000 Gt C [*Beerling and Brentnall*, 2007].

[39] The Karoo sediments contain substantial amount of coal deposits in the Ecca, Beaufort and Stormberg groups (Figure 3), in the Main Karoo basin and in other Karoo basins as well throughout southern Africa (e.g., Kalahari, Tuli and Save basins) (Figure 2a) [*Cairncross*, 2001]. All these formations are more or less densely intruded by sills all over the Karoo basins (e.g., Figures 1 and 2). Theoretically, the carbon contained in the sediments is partially converted into methane when temperature reaches 100–200°C at contact with the magma [*Svensen et al.*, 2004, 2007].

Evidence is found in the various coal ranks observed for the Karoo Ecca coal which ranges from highly volatile bituminous to degassed anthracite, the latter being strong support of overprinted thermal metamorphism signature and attendant methane and CO_2 degassing [*Snyman and Barclay*, 1989; *Catuneanu et al.*, 2005]. In addition, evidence for a substantial amount of gas has been found in the north central part of the Main Karoo basin [*Catuneanu et al.*, 2005]. Altogether, this suggests that these C-rich layers would be a significant methane and CO_2 source of light carbon (~2000–7500 Gt C [*Svensen et al.*, 2007]). These coal formations also contain ~1–2% of sulphur [*Cairncross*, 2001] that can be responsible for a short initial cooling and deforestation by acid rains [*Self et al.*, 2005]. The methane and CO_2 (and SO_2) have been proposed to be vertically transported to the surface by thousands of hydrothermal pipes and vents complexes documented throughout the Main Karoo sedimentary basin [*Svensen et al.*, 2004, 2006a, 2007]. No radioisotopic dates are available for these specific events, but at least some of them occurred early, before the Lesotho lava-pile emplacement (181.6 ± 0.7 Ma [*Jourdan et al.*, 2007b]), as attested by pipe-related deposits in the Clarens formation [*Ross et al.*, 2005; *Svensen et al.*, 2006a] (Figure 2). Calibrated $^{40}Ar/^{39}Ar$ and U/Pb ages obtained on eighteen sills intruding the Karoo sediments of the three major basins [*Encarnacion et al.*, 1996; *Duncan et al.*, 1997; *Jourdan et al.*, 2005; *Svensen et al.*, 2007; this study] are in accordance with an intrusive activity starting very early in the history of the Karoo LIP and then becoming more protracted for a few million years (Figure 6c). Therefore, those data suggest either (1) that if the hydrothermal pipes were synchronous with the sill injections, then they were formed over a few million years (~3 ± 1 Ma) or (2) that the pipes might have been erupted in much shorter period of time provided that the sedimentary basin acts as a time buffer and requires a certain threshold of gas pressure in the low-permeability sediments before the pipes can erupt. Ultimately, further modeling that would test the viability of the gas pressure threshold hypothesis needs to be undertaken. Ideally, direct dating of the pipe emplacement would shed some light on this possibility.

[40] In summary, CO_2 and CH_4 released from Karoo large volcanic eruptions and repeated injections of magma into C-rich sedimentary layers, and subsequently from gas hydrate reservoirs buried in seafloor sediments (due to an increase of ambient temperature), provide a viable mechanism for climate destabilization, especially when the three sources are combined together. In addition, volcanogenic and coal-derived SO_2 emissions are likely to be a significant factor as well, although acting on a much shorter scale [*Self et al.*, 2006]. In the case of the Karoo magmatism, the apparent age of the increase of eruption rate and the intrusions in the C-rich layers nicely coincides with the age of the Pliensbachian-Toarcian boundary and related isotopic excursions.

5.2.4. Why Only a Minor Mass Extinction?

[41] The Karoo magma erupted following two different schemes. The first one consists of brief and temporally distinct magmatic pulses contributing significantly to the total volume of the province (e.g., Lesotho and southern Botswana lava piles). The second one is represented by a more diffuse but persistent magmatism (also representing a large volume; e.g., the sills) that lasted for a few million years. Therefore, considering the short lifetime of the SO_2 in the atmosphere (a few years for a single input) and the ability of CO_2 and CH_4 to equilibrate relatively rapidly compared to the relatively low eruption rate of the magma [*Wignall*, 2001] (Figure 7c), this would leave enough time for the ecosystem to recover between each individual volcanic event and gradual climate change. This is true even if (1) important additional volumes of volatiles are provided by coal-rich sedimentary layers as their release is spread over a protracted period and (2) some large volumes of magma such as the Lesotho lava pile are emplaced in a brief time span (<0.8 Ma [*Jourdan et al.*, 2007b]) as they individually contribute only to relatively moderate fraction of the total volcanogenic volume of volatiles. Following our previous statement [*Jourdan et al.*, 2005], the timing of eruptions and the time span between each event may be among the most compelling factors that control the impact of the CFB on an ecosystem. This proposition is in accordance with modeling by *Beerling and Brentnall* [2007], who showed that long-term volcanogenic and coal related CO_2 and CH_4 emissions do not significantly alter the climate if they are spread over few million of years, and thus are less likely to trigger a massive mass extinction.

[42] In the case of the Karoo province, the relatively low eruption rates may explain the absence of a more *severe* mass extinction at the Pliensbachian-Toarcian boundary, compared to other short-lasting large igneous provinces synchronous with more severe biota disruption (e.g., Siberian traps at the

Permo-Triassic boundary [*Renne et al.*, 1995; *Reichow et al.*, 2002]). Other limiting factors such as the low latitude of southern Africa at this time and the absence of more explosive magmatism (i.e., pyroclastic eruption [*Reichow et al.*, 2002]) might also have played a crucial role as buffer effect in the injection of the volatiles in the stratosphere.

6. Conclusion

[43] From the voluminous southern sill complex of the Main Karoo basin, we analyzed fifteen samples and obtained nine plateau and four miniplateau ages including nine geologically robust ages ranging from 176.2 ± 1.3 to 183.8 ± 2.4 Ma with all but one age ranging between 181 and 184 Ma. Critical and careful combination of age data from the sill complex and other parts of the province allows us drawing the following conclusions:

[44] 1. The abundant sills from southeastern South Africa do not represent a brief magmatic event in the Karoo province, as previously proposed, but rather were emplaced over ~2–3 Ma. Emplacement duration of the sills mimics the behavior of the main activity of the province with a relatively diffuse and protracted activity. These ages confirm that the main volume of the Karoo LIP was not emplaced in <1 Ma but rather on a longer time span (4 ± 1 Ma).

[45] 2. One sill and two dikes from the Underberg dike swarm suggest the occurrence of a late stage basaltic activity at ~176 Ma near the southern continental rifted margin. The ascent of the magma at this time could have been facilitated by the distention occurring in this region as previously suggested for the silicic and MORB-like magmatism along the Lebombo region.

[46] 3. The age of the Pliensbachian-Toarcian minor biotic crisis coincides closely with an increase of magmatic productivity of the Karoo LIP, provided that appropriate intercalibrations between the $^{40}Ar/^{39}Ar$ and U-Pb chronometers are considered. Considering recent estimates of $\delta^{13}C$ mantle value, volcanogenic CO_2 (and SO_2) emissions could be ones of the main culprits responsible for the Pliensbachian-Toarcian climate perturbation. The Toarcian oceanic anoxic event could be linked to the long lasting Karoo igneous activity. Precise dating of the Pliensbachian-Toarcian boundary and better calibration of the ^{40}K decay constant are required to precisely pinpoint synchrony of the Karoo LIP emplacement and climate change.

[47] 4. The sills intruded the coal-bearing sedimentary layers throughout southern Africa. These C-rich layers can provide a substantial amount of methane, CO_2 and SO_2 at contact with the magma intruding the basin. The gas is further transported to the surface by the mean of pipes. We propose two distinct hypotheses whereby (1) the pipe eruptions would be in step with the sill injections over a few Ma or (2) the sedimentary basin need to reach a gas saturation pressure threshold before the gas can be vented at the surface, over a much shorter time span. In both case, the coal-derived CH_4, CO_2 and SO_2 could represent important factors in the Pliensbachian-Toarcian climate perturbation as well. Both volcanogenic- and coal-derived C could have triggered initial global warming subsequently allowing the thermogenically driven release of CH_4 contained in gas hydrate reservoirs.

[48] 5. Contrary to some massive mass extinctions apparently related to other LIPs, the Pliensbachian-Toarcian event is a second-order crisis where "only" 5% of the families have been wiped out. This lower impact of the Karoo LIP on the biosphere may be related to the protracted igneous activity (i.e., with relatively low eruption rates), occurring both as volcanic emissions and as intrusions within C-rich layers. In this case, the atmosphere and ocean would have sufficient time to recover, at least partly, between each eruption pulse. The low-latitude position of southern Africa at this time and rarity of explosive-type volcanism might also have been unfavorable to a severe perturbation.

Acknowledgments

[49] This work is part of a collaboration between the University of Kwazulu-Natal (Durban), the Universities of Nice and Lyon, and the Berkeley Geochronology Center. We acknowledge the financial support of the CNRS-PICS program. This study was also supported by NSF grant EAR-9909517 and the Ann and Gordon Getty Foundation. M. Manetti and T. A. Becker are thanked for analytical assistance. H. Svensen and an anonymous reviewer are thanked for reviewing a previous version of the manuscript. Formal reviews by A. Marzoli and W. Hames are acknowledged.

References

Bailey, T. R., Y. Rosenthal, J. M. McArthur, B. van de Schootbrugge, and M. F. Thirlwall (2003), Paleoceanographic changes of the Late Pliensbachian–Early Toarcian interval: A possible link to the genesis of an Oceanic Anoxic Event, *Earth Planet. Sci. Lett.*, *212*, 307–320, doi:10.1016/S0012-821X(03)00278-4.

Beerling, D. J., and R. A. Berner (2002), Biogeochemical constraints on the Triassic-Jurassic boundary carbon cycle event, *Global Biogeochem. Cycles*, *16*(3), 1036, doi:10.1029/2001GB001637.

Beerling, D. J., and S. J. Brentnall (2007), Numerical evaluation of mechanisms driving Early Jurassic changes in global carbon cycling, *Geology*, *35*, 247–250, doi:10.1130/G23416A.1.

Cairncross, B. (2001), An overview of the Permian (Karoo) coal deposits of southern Africa, *J. Afr. Earth Sci.*, *33*, 529–562, doi:10.1016/S0899-5362(01)00088-4.

Catuneanu, O., H. Wopfner, P. G. Eriksson, B. Cairncross, B. S. Rubidge, R. M. H. Smith, and P. J. Hancox (2005), The Karoo basins of south-central Africa, *J. Afr. Earth Sci.*, *43*, 211–253, doi:10.1016/j.jafrearsci.2005.07.007.

Chevallier, L., and A. C. Woodford (1999), Morpho-tectonics and mechanism of emplacement of dolerite rings and sills of western Karoo, South Africa, *S. Afr. J. Geol.*, *102*, 43–54.

Courtillot, V. E., and P. R. Renne (2003), On the ages of flood basalt events, *C. R. Geosci.*, *335*, 113–140, doi:10.1016/S1631-0713(03)00006-3.

Cox, K. G. (1988), The Karoo Province, in *Continental Flood Basalts*, edited by J. D. MacDougall, pp. 239–271, Springer, New York.

De Min, A., E. M. Piccirillo, A. Marzoli, G. Bellieni, P. R. Renne, M. Ernesto, and L. S. Marques (2002), The Central Atlantic Magmatic Province in Brazil: Petrogenesis, $^{40}Ar/^{39}Ar$ ages, paleomagnetism and geodynamic implications, in *The Central Atlantic Magmatic Province: Insights From Fragments of Pangea*, *Geophys. Monogr. Ser.*, vol. 136, edited by W. E. Hames et al., pp. 91–128, AGU, Washington, D. C.

Deines, P. (2002), The carbon isotope geochemistry of mantle xenoliths, *Earth Sci. Rev.*, *58*, 247–278, doi:10.1016/S0012-8252(02)00064-8.

Duncan, A. R., R. A. Armstong, A. J. Erlank, J. S. Marsh, and R. T. Watkins (1990), MORB-related dolerites associated with the final phases of Karoo flood basalt volcanism in southern Africa, in *Mafic Dikes and Emplacement Mechanisms*, edited by A. J. Parker, P. C. Rickwood, and D. H. Tucker, pp. 119–129, A. A. Balkema, Brookfield, Vt.

Duncan, R. A., P. R. Hooper, J. Rehacek, J. S. Marsh, and A. R. Duncan (1997), The timing and duration of the Karoo igneous event, southern Gondwana, *J. Geophys. Res.*, *102*, 18,127–18,138, doi:10.1029/97JB00972.

Encarnacion, J., T. H. Fleming, H. Elliot, and H. V. Eales (1996), Synchronous emplacement of Ferrar and Karoo dolerites and the early breakup of Gondwana, *Geology*, *24*, 535–538, doi:10.1130/0091-7613(1996)024<0535:SEOFAK>2.3.CO;2.

Fuentes, F., G. Féraud, L. Aguirre, and D. Morata (2005), $^{40}Ar/^{39}Ar$ dating of volcanism and subsequent very low-grade metamorphism in a subsiding basin: Example of the Cretaceous lava series from central Chile, *Chem. Geol.*, *214*, 157–177, doi:10.1016/j.chemgeo.2004.09.001.

Gérard, M., S. Caquineau, A. L. Chenet, F. Fluteau, V. Courtillot, and K. V. Subbarao (2006), Red boles in the Deccan traps: Time constraints from alteration processes, *Geophys. Res. Abstr.*, *8*, Abstract 07092.

Gradstein, F. M., et al. (2004), A geological time scale 2004, Int. Comm. on Stratigr., Oslo. (Available at http://www.stratigraphy.org)

Hansen, H. J. (2006), Stable isotopes from basaltic rocks and their possible relation to atmospheric isotope excursions, *Lithos*, *92*, 105–116, doi:10.1016/j.lithos.2006.03.029.

Heizler, M. T., and T. M. Harrison (1988), Multiple trapped argon isotope components revealed by $^{40}Ar/^{39}Ar$ isochron analysis, *Geochim. Cosmochim. Acta*, *52*, 1295–1303, doi:10.1016/0016-7037(88)90283-9.

Hofmann, C., G. Féraud, and V. Courtillot (2000), $^{40}Ar/^{39}Ar$ dating of mineral separates and whole rocks from the Western Ghats lava pile: Further constraints on duration and age of the Deccan traps, *Earth Planet. Sci. Lett.*, *180*, 13–27, doi:10.1016/S0012-821X(00)00159-X.

Jones, D. L., R. A. Duncan, J. C. Briden, D. E. Randall, and C. MacNiocaill (2001), Age of the Batoka basalts, northern Zimbabwe, and the duration of Karoo Large Igneous Province magmatism, *Geochem. Geophys. Geosyst.*, *2*(2), 1022, doi:10.1029/2000GC000110.

Jourdan, F., and P. R. Renne (2007), Age calibration of the Fish Canyon sanidine $^{40}Ar/^{39}Ar$ dating standard using primary K-Ar standards, *Geochim. Cosmochim. Acta*, *71*, 387–402, doi:10.1016/j.gca.2006.09.002.

Jourdan, F., G. Féraud, H. Bertrand, A. B. Kampunzu, G. Tshoso, B. Le Gall, J. J. Tiercelin, and P. Capiez (2004), The Karoo triple junction questioned: Evidence from $^{40}Ar/^{39}Ar$ Jurassic and Proterozoic ages and geochemistry of the Okavango dike swarm (Botswana), *Earth Planet. Sci. Lett.*, *222*, 989–1006, doi:10.1016/j.epsl.2004.03.017.

Jourdan, F., G. Féraud, H. Bertrand, A. B. Kampunzu, G. Tshoso, M. K. Watkeys, and B. Le Gall (2005), The Karoo large igneous province: Brevity, origin, and relation with mass extinction questioned by new $^{40}Ar/^{39}Ar$ age data, *Geology*, *33*, 745–748, doi:10.1130/G21632.1.

Jourdan, F., C. Verati, and G. Féraud (2006), Intercalibration of the Hb3gr $^{40}Ar/^{39}Ar$ dating standard, *Chem. Geol.*, *231*, 177–189, doi:10.1016/j.chemgeo.2006.01.027.

Jourdan, F., G. Féraud, H. Bertrand, and M. K. Watkeys (2007a), From flood basalts to the inception of oceanization: Example from the $^{40}Ar/^{39}Ar$ high-resolution picture of the Karoo large igneous province, *Geochem. Geophys. Geosyst.*, *8*, Q02002, doi:10.1029/2006GC001392.

Jourdan, F., G. Féraud, H. Bertrand, M. K. Watkeys, and P. R. Renne (2007b), Distinct brief major events in the Karoo large igneous province clarified by new $^{40}Ar/^{39}Ar$ ages on the Lesotho basalts, *Lithos*, *98*, 195–209, doi:10.1016/j.lithos.2007.03.002.

Jourdan, F., J. P. Matzel, and P. R. Renne (2007c), Direct measurement of ^{39}Ar (and ^{37}Ar) recoil ejection during neutron irradiation of sanidine and plagioclase crystals, *Geochim. Cosmochim. Acta*, *71*, 2791–2808, doi:10.1016/j.gca.2007.03.017.

Kattenhorn, S. A., and M. K. Watkeys (1995), Some revelations from Karoo dolerite sills, west of Empangeni, KwaZulu-Natal, *Petros*, *14*, 1–16.

Kelley, S. (2002), Excess argon in K-Ar and Ar-Ar geochronology, *Chem. Geol.*, *188*, 1–22, doi:10.1016/S0009-2541(02)00064-5.

Kwon, J., K. Min, P. Bickel, and P. R. Renne (2002), Statistical methods for jointly estimating decay constant of ^{40}K and age of a dating standard, *Math. Geol.*, *34*, 457–474, doi:10.1023/A:1015035228810.

Landoll, J. D., K. A. Foland, and C. M. B. Henderson (1989), Excess argon in amphiboles from fluid interaction and short intrusion interval at the epizonal Marangudzi complex, Zimbabwe, *J. Geophys. Res.*, *94*, 4053–4069.

Le Gall, B., G. Tshoso, F. Jourdan, G. Féraud, H. Bertrand, J. J. Tiercelin, A. B. Kampunzu, M. P. Modisi, M. Dyment, and J. Maia (2002), $^{40}Ar/^{39}Ar$ geochronology and structural

data from the giant Okavango and related mafic dike swarms, Karoo igneous province, Botswana, *Earth Planet. Sci. Lett.*, *202*, 595–606, doi:10.1016/S0012-821X(02)00763-X.

Le Gall, B., G. Tshoso, J. Dyment, A. B. Kampunzu, F. Jourdan, G. Féraud, H. Bertrand, and C. Aubourg (2005), The Okavango giant mafic dike swarm (NE Botswana) and its structural significance within the Karoo Large Igneous Province, *J. Struct. Geol.*, *27*, 2234–2255, doi:10.1016/j.jsg.2005.07.004.

Little, C. T. S., and M. J. Benton (1995), Early Jurassic mass extinction: A global long-term event, *Geology*, *23*, 495–498, doi:10.1130/0091-7613(1995)023<0495:EJMEAG>2.3.CO;2.

Marsh, J. S., P. R. Hooper, J. Rehacek, R. A. Duncan, and A. R. Duncan (1997), Stratigraphy and age of Karoo basalts of Lesotho and implications for correlation within the Karoo igneous province, in *Large Igneous Provinces: Continental, Oceanic, and Planetary Flood Volcanism*, *Geophys. Monogr. Ser.*, vol. 100, edited by J. J. Mahoney and M. F. Coffin, pp. 247–272, AGU, Washington, D. C.

McElwain, J. C., J. Wade-Murphy, and S. P. Hesselbo (2005), Changes carbon dioxide during an oceanic anoxic event linked to into Gondwana coals, *Nature*, *435*, 479–482, doi:10.1038/nature03618.

Merrihue, C., and G. Turner (1966), Potassium-argon dating by activation with fast neutrons, *J. Geophys. Res.*, *71*, 2852–2857.

Min, K., R. Mundil, P. R. Renne, and K. R. Ludwig (2000), A test for systematic errors in ^{40}Ar/^{39}Ar geochronology through comparison with U-Pb analysis of a 1.1 Ga rhyolite, *Geochim. Cosmochim. Acta*, *64*, 73–98, doi:10.1016/S0016-7037(99)00204-5.

Mundil, R., P. R. Renne, K. K. Min, and K. R. Ludwig (2006), Resolvable miscalibration of the ^{40}Ar/^{39}Ar geochronometer, *Eos Trans. AGU*, *87*(52), Fall Meet. Suppl., Abstract V21A-0543.

Nomade, S., P. R. Renne, and R. K. W. Merkle (2004), ^{40}Ar/^{39}Ar age constraints on ore deposition and cooling of the Bushveld Complex, South Africa, *J. Geol. Soc.*, *161*, 411–420.

Paine, J. H., S. Nomade, and P. R. Renne (2006), Quantification of ^{39}Ar recoil ejection from GA1550 biotite during neutron irradiation as a function of grain dimensions, *Geochim. Cosmochim. Acta*, *70*, 1507–1517, doi:10.1016/j.gca.2005.11.012.

Pálfy, J., and P. L. Smith (2000), Synchrony between Early Jurassic extinction, oceanic anoxic event, and the Karoo-Ferrar flood basalt volcanism, *Geology*, *28*, 747–750, doi:10.1130/0091-7613(2000)28<747:SBEJEO>2.0.CO;2.

Polteau, S., A. Mazzini, O. Galland, S. Planke, and A. Malthe-Sorenssen (2008), Saucer-shaped intrusions: Occurrences, emplacement and implications, *Earth Planet. Sci. Lett.*, *266*, 195–204.

Reichow, M. K., A. D. Saunders, R. V. White, M. S. Pringle, A. I. Mukhamedov, A. I. Medevev, and N. P. Kirda (2002), ^{40}Ar/^{39}Ar dates from the west Siberian Basin: Siberian flood basalt province doubled, *Science*, *296*, 1846–1849, doi:10.1126/science.1071671.

Renne, P. R., Z. Zichao, M. A. Richards, M. T. Black, and A. R. Basu (1995), Synchrony and causal relations between Permian-Triassic boundary crises and Siberian flood volcanism, *Science*, *269*, 1413–1416, doi:10.1126/science.269.5229.1413.

Renne, P. R., W. D. Sharp, A. L. Deino, G. Orsi, and L. Civetta (1997), ^{40}Ar/^{39}Ar dating into historical realm: Calibration against Pliny the Younger, *Science*, *277*, 1279–1280, doi:10.1126/science.277.5330.1279.

Renne, P. R., C. C. Swisher, A. L. Deino, D. B. Karner, T. Owens, and D. J. Depaolo (1998), Intercalibration of standards, absolute ages and uncertainties in ^{40}Ar/^{39}Ar dating, *Chem. Geol.*, *145*, 117–152, doi:10.1016/S0009-2541(97)00159-9.

Riley, T. R., L. Milar, M. K. Watkeys, M. L. Curtis, P. T. Leat, M. B. Klausen, and C. M. Fanning (2004), U-Pb Zircon (SHRIMP) ages for the Lebombo rhyolites, South Africa: Refining the duration of Karoo volcanism, *J. Geol. Soc.*, *161*, 547–550, doi:10.1144/0016-764903-181.

Riley, T. R., M. L. Curtis, P. T. Leat, M. K. Watkeys, R. A. Duncan, I. L. Millar, and W. H. Owens (2006), Overlap of Karoo and Ferrar magma types in KwaZulu-Natal, South Africa, *J. Petrol.*, *47*, 541–566, doi:10.1093/petrology/egi085.

Roddick, J. C. (1978), The application of isochron diagrams in ^{40}Ar-^{39}Ar dating: A discussion, *Earth Planet. Sci. Lett.*, *41*, 233–244, doi:10.1016/0012-821X(78)90014-6.

Ross, P.-S., I. Ukstins Peate, Y. G. McClintock, Y. G. Xu, I. P. Skilling, J. D. L. White, and B. F. Houghton (2005), Mafic volcaniclastic deposits in flood basalt provinces: A review, *J. Volcanol. Geotherm. Res.*, *145*, 281–314, doi:10.1016/j.jvolgeores.2005.02.003.

Rosset, A., A. De Min, L. S. Marques, M. J. B. Macambira, M. Ernesto, P. R. Renne, and E. M. Piccirillo (2007), Genesis and geodynamic significance of Mesoproterozoic and Early Cretaceous tholeiitic dike swarms from the São Francisco craton (Brazil), *J. South Am. Earth Sci.*, *24*, 69–92, doi:10.1016/j.jsames.2007.02.002.

Roswell, D. M., and A. M. J. De Sward (1976), Diagenesis in Cape and Karoo sediments, South Africa and its bearing on their hydrocarbon potential, *Trans. Geol. Soc. S. Afr.*, *79*, 81–145.

Self, S., T. Thordarson, and M. Widdowson (2005), Gas fluxes from flood basalt eruption, *Elements*, *1*, 283–287, doi:10.2113/gselements.1.5.283.

Self, S., M. Widdowson, T. Thordarson, and E. A. Jay (2006), Volatile fluxes during flood basalt eruptions and potential effects on the global environment: A Deccan perspective, *Earth Planet. Sci. Lett.*, *248*, 518–532, doi:10.1016/j.epsl.2006.05.041.

Sharp, W. D., and P. R. Renne (2005), The ^{40}Ar/^{39}Ar dating of core recovered by the Hawaii Scientific Drilling Project (phase 2), Hilo, Hawaii, *Geochem. Geophys. Geosyst.*, *6*, Q04G17, doi:10.1029/2004GC000846.

Sircombe, K. N. (2004), AgeDisplay: An EXCEL workbook to evaluate and display univariate geochronological data using binned frequency histograms and probability density distributions, *Comput. Geosci.*, *30*, 21–31, doi:10.1016/j.cageo.2003.09.006.

Snyman, C. P., and J. Barclay (1989), The coalification of South African coal, *Int. J. Coal Geol.*, *13*, 375–390, doi:10.1016/0166-5162(89)90100-6.

Steiger, R. H., and E. Jager (1977), Subcommission on geochronology: Convention of the use of decay constants in geo- and cosmochronology, *Earth Planet. Sci. Lett.*, *36*, 359–362, doi:10.1016/0012-821X(77)90060-7.

Suan, G., B. Pittet, I. Bour, E. Mattioli, L. V. Duarte, and S. Mailliot (2008), Duration of the Early Toarcian carbon isotope excursion deduced from spectral analysis: Consequence for its possible causes, *Earth Planet. Sci. Lett.*, *267*, 666–679, doi:10.1016/j.epsl.2007.12.017.

Svensen, H., S. Planke, A. Malthe-Sorensssen, B. Jamtveit, R. Myklebust, T. R. Eidem, and S. Rey (2004), Release of

methane from a volcanic basin as a mechanism for initial Eocene global warming, *Nature*, *429*, 542–545, doi:10.1038/nature02566.

Svensen, H., B. Jamtveit, S. Planke, and L. Chevallier (2006a), Structure and evolution of hydrothermal vents complexes in the Karoo basin, South Africa, *J. Geol. Soc.*, *163*, 671–682, doi:10.1144/1144-764905-037.

Svensen, H., S. Planke, A. Polozov, and N. Schmidbauer (2006b), Magma-salt interactions and degassing from the Tunguska basin, Siberia: Towards a new killer model for the P-Tr mass extinction, *Eos Trans. AGU*, *87*(52), Fall Meet. Suppl., Abstract V53A-1744.

Svensen, H., S. Planke, L. Chevallier, A. Malthe-Sørenssen, F. Corfu, and B. Jamtveit (2007), Hydrothermal venting of greenhouse gases triggering Early Jurassic global warming, *Earth Planet. Sci. Lett.*, *256*, 554–566, doi:10.1016/j.epsl.2007.02.013.

Turner, B. R. (1999), Tectonostratigraphical development of the Upper Karoo foreland basin: Orogenic unloading versus thermally-induced Gondwana rifting, *J. Afr. Earth Sci.*, *28*, 215–238, doi:10.1016/S0899-5362(99)00025-1.

Turner, G., J. C. Huneke, F. A. Podose, and G. J. Wasserbrug (1971), $^{40}Ar/^{39}Ar$ ages and cosmic ray exposure ages of Apollo 14 samples, *Earth Planet. Sci. Lett.*, *12*, 19–35, doi:10.1016/0012-821X(71)90051-3.

van de Schootbrugge, B., J. M. McArthur, T. R. Bailey, Y. Rosenthal, J. D. Wright, and K. G. Miller (2005), Toarcian oceanic anoxic event: An assessment of global causes using belemnite C isotope records, *Paleoceanography*, *20*, PA3008, doi:10.1029/2004PA001102.

Verati, C., and G. Féraud (2003), Ar-Ar plateau ages disturbed by minor alteration phases in plagioclases: How to assess the true duration of brief volcanic events, *Geophys. Res. Abstr.*, *5*, Abstract 06356.

Wignall, P. (2001), Large igneous provinces and mass extinctions, *Earth Sci. Rev.*, *53*, 1–33, doi:10.1016/S0012-8252(00)00037-4.

Wignall, P. (2005), The link between large igneous province eruptions and mass extinction, *Elements*, *1*, 293–297, doi:10.2113/gselements.1.5.293.